Available online at www.sciencedirect.com
SCIENCE DIRECT
International Journal of Hydrogen Energy 31 (2006) 1182–1187
International Journal of HYDROGEN ENERGY
www.elsevier.com/locate/ijhydene

Phase relations and electrochemical properties of $Ca_{1-x}Mg_x(Ni_{0.9}Al_{0.1})_2$ alloys

Q.A. Zhang*, G.P. Zhao, T.Z. Si

School of Materials Science and Engineering, Anhui University of Technology, Maanshan, Anhui 243002, PR China

Available online 25 October 2005

Abstract

The phase relations and electrochemical properties of the $Ca_{1-x}Mg_x(Ni_{0.9}Al_{0.1})_2$ alloys have been studied. It was found that the single C15 phase and the single C36 phase exist, respectively, in the approximate composition ranges of $x = 0$–0.63 and 0.76–1. Between the single-phase regions, the C15 and C36 phases coexist. The hydrogen storage capacity of the C15-type $Ca_{1-x}Mg_x(Ni_{0.9}Al_{0.1})_2$ alloys was lifted with increasing Mg content x. When $x = 0.6$, the hydrogen absorption and desorption capacities are 1.33 and 0.8 wt%, respectively. The alloy electrodes do not need activation during electrochemical measurements. The discharge capacity of the $Ca_{0.4}Mg_{0.6}(Ni_{0.9}Al_{0.1})_2$ alloy is 401 mAh/g at a discharge current of 10 mA/g. However, the cyclic stability should be improved significantly.

Keywords: Hydrogen absorbing materials; Crystal structure; Electrochemical property

1. Introduction

Recently new hydrogen absorbing materials with light elements have been developed to increase hydrogen storage capacity. For examples, aluminum-containing hydrides such as $NaAlH_4$, $LiAlH_4$, Sr_2AlH_7, $BaAlH_5$ and Ba_2AlH_7 have been extensively studied for this purpose [1–9]. In the meantime, Mg-based alloys have also attracted more attention due to their high hydrogen storage capacities [10,11]. Furthermore, several La–Mg–Ni system alloys have been successfully developed for electrode materials in nickel/metal hydride (Ni/MH) batteries because of their good electrochemical properties [12–15].

Ca–Ni-based alloys with low densities are also candidates for hydrogen storage applications. For example, $CaNi_5$ has a hydrogen storage capacity of 1.9 wt% [16]. $Ca_{0.4}Mg_{0.6}Ni_3$ alloy with the $PuNi_3$ structure can absorb 1.56 wt% of hydrogen at room temperature [17–19]. The crystal structures and hydrogen storage properties of $Ca_{1-x}Mg_xNi_2$ alloys were first reported by Oesterreicher [20], which were further investigated by Terashita [21]. $CaNi_2$ is a C15-type Laves phase and $MgNi_2$ is a C36-type Laves phase. Terashita found that the single C15 Laves phase existed in the composition range between $CaNi_2$ and $Ca_{0.32}Mg_{0.68}Ni_2$, and the maximum hydrogen content was 1.4 wt% at 313 K [21].

The purpose of this work is to investigate the possible application of the $Ca_{1-x}Mg_xNi_2$-based alloys for electrode materials in Ni/MH batteries. In order to increase the corrosion resistance of the alloys in KOH electrolyte solution and improve their charge–discharge

* Corresponding author. Tel.: +86 555 2400615; fax: +86 555 2471263.
E-mail address: zhang03jp@yahoo.com.cn (Q.A. Zhang).

0360-3199/$30.00
doi:10.1016/j.ijhydene.2005.09.006

cycle life, we have selected $Ca_{1-x}Mg_x(Ni_{0.9}Al_{0.1})_2$ alloys as the investigated materials. However, the partial substitution of Ni by Al would lead to a change in crystal structure and hydrogen storage property. Thus we have studied the crystal structure, hydrogen absorption/desorption properties and electrochemical properties of $Ca_{1-x}Mg_x(Ni_{0.9}Al_{0.1})_2$ alloys in this work.

2. Experimental details

The $Ca_{1-x}Mg_x(Ni_{0.9}Al_{0.1})_2$ ($x = 0$, 0.3, 0.4, 0.5, 0.6, 0.7, 0.8 and 1.0) alloys were prepared by magnetic levitation melting of appropriate amounts of pure metals. The samples were remelted three times to ensure homogeneity. Before the preparation, the losses of Ca and Mg during melting were determined to be about 3 and 10 wt%, respectively. On the basis of stoichiometric amounts of starting materials, thus, extra 3 wt% of Ca and 10 wt% of Mg were added to compensate the losses of Ca and Mg during melting. The ingots were wrapped in tantalum sheets, placed in stainless steel autoclaves under argon atmosphere and annealed at 973 K for 7 days.

The alloys were first ground to powders with particle size smaller than 45 μm in a glove box under dry argon atmosphere. The powder samples were then loaded into stainless steel autoclaves. The pressure–composition (P–C) isotherms were measured using a Sietverts-type apparatus at 313 K. Before the measurements, the samples were activated by the following process. The powder samples in the autoclaves were evacuated at 373 K for 1 h. Then they were hydrogenated under a hydrogen pressure of 3 MPa for 1 h, followed by three hydriding–dehydriding cycles at 373 K and finally cooling down to 313 K.

In order to evaluate the phase structures of the samples, X-ray diffraction (XRD) measurements were performed using a Rigaku D/MAX-3B diffractometer with Cu Kα radiation at 40 kV and 30 mA. The XRD profiles were analyzed with the Rietveld refinement program RIETAN-2000 [22].

All test electrodes were prepared by mixing alloy powders with copper powder in a weight ratio of 1:2 and then cold-pressing the mixture into pellets. The electrochemical measurements on test electrodes were conducted at 298 K with a sintered $Ni(OH)_2$/NiOOH positive counter electrode and a Hg/HgO (6 N KOH) reference electrode. The test electrodes were charged at 100 mA/g for 6 h and discharged at different currents to the cut-off potential of −0.6 V vs. Hg/HgO reference electrode.

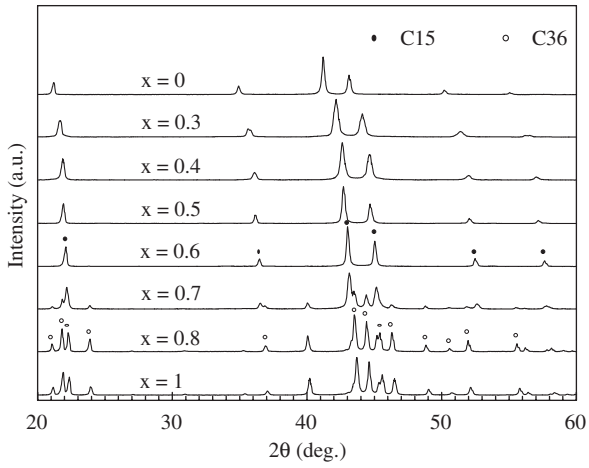

Fig. 1. X-ray diffraction patterns for $Ca_{1-x}Mg_x(Ni_{0.9}Al_{0.1})_2$ alloys.

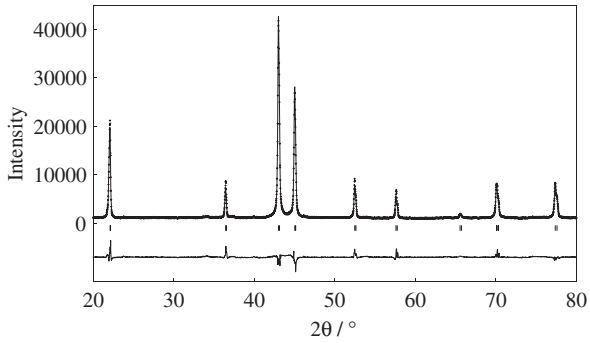

Fig. 2. Calculated (line) and observed (+) X-ray diffraction patterns for the $Ca_{0.4}Mg_{0.6}(Ni_{0.9}Al_{0.1})_2$ alloy. Vertical bars below the patterns show the positions of all possible reflection peaks of the C15 phase. The difference between the observed and calculated patterns is shown below the vertical bars.

3. Results and discussion

Fig. 1 shows the XRD patterns of the $Ca_{1-x}Mg_x(Ni_{0.9}Al_{0.1})_2$ ($x = 0$, 0.3, 0.4, 0.5, 0.6, 0.7, 0.8 and 1.0) alloys. It can be seen that a single C15 Laves phase is present when x is in the range from 0 to 0.6. The XRD peaks of the C15 phase shift to higher 2θ values with increasing x, indicating that the lattice parameter decreases with the increase of Mg content. Increasing x to 0.7, the alloy consists of C15 and C36 phases. However, only a single C36 phase can be found in the alloy with $x = 0.8$.

In order to calculate the lattice parameters and phase abundance, the XRD profiles were refined by the Rietveld method. Fig. 2 shows the result of the Rietveld analysis for the $Ca_{0.4}Mg_{0.6}(Ni_{0.9}Al_{0.1})_2$ alloy. For the Rietveld refinement, the structure model for the C15 phase was taken from the reported structure for $CaNi_2$

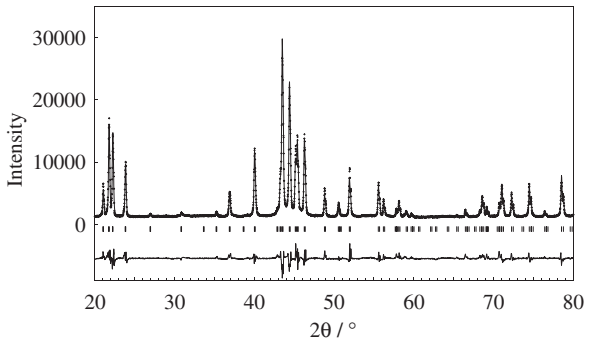

Fig. 3. Calculated (line) and observed (+) X-ray diffraction patterns for the $Ca_{0.2}Mg_{0.8}(Ni_{0.9}Al_{0.1})_2$ alloy. Vertical bars below the patterns show the positions of all possible reflection peaks of the C36 phase. The difference between the observed and calculated patterns is shown below the vertical bars.

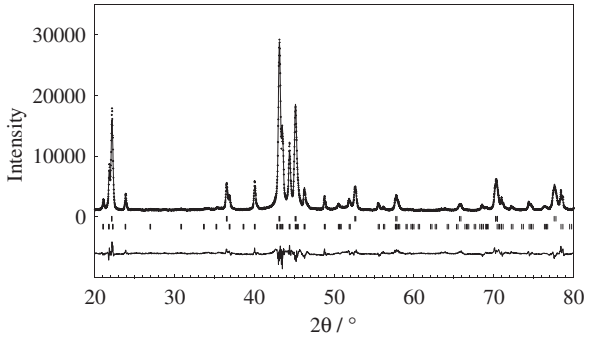

Fig. 4. Calculated (line) and observed (+) X-ray diffraction patterns for the $Ca_{0.3}Mg_{0.7}(Ni_{0.9}Al_{0.1})_2$ alloy. Vertical bars below the patterns show the positions of all possible reflection peaks of the C15 and C36 phases (from above), respectively. The difference between the observed and calculated patterns is shown below the vertical bars.

[23]. We assumed that Mg and Al atoms occupy the Ca and Ni sites, respectively. Fig. 3 presents the result of the Rietveld analysis for the $Ca_{0.2}Mg_{0.8}(Ni_{0.9}Al_{0.1})_2$ alloy. The structure model for the C36 phase was taken from the reported structure for $MgNi_2$ [24]. Similarly, we assumed that Ca and Al atoms, respectively, occupy the Mg and Ni sites. As shown in Figs. 2 and 3, the diffraction patterns calculated from the structure models are in good agreement with those measured.

The calculated and observed XRD patterns for the $Ca_{0.3}Mg_{0.7}(Ni_{0.9}Al_{0.1})_2$ alloy are shown in Fig. 4. The C15 and C36 phases were calculated to be 52 and 48 wt%, respectively. The crystal structural parameters and phase abundance of the $Ca_{1-x}Mg_x(Ni_{0.9}Al_{0.1})_2$ ($x = 0$, 0.3, 0.4, 0.5, 0.6, 0.7, 0.8 and 1.0) alloys were summarized in Table 1. It can be seen that the lattice parameters of the C15 and C36 phases decrease with increasing Mg content x. Fig. 5 shows the relationship between the lattice parameter a and x. Assuming that the lattice parameters of the C15 or C36 phases in the single-phase alloys have a linear relationship to x and those of the C15 and C36 phases in the double-phase alloys keep constant, the maximum solubility of Mg in the C15 phase $Ca(Ni_{0.9}Al_{0.1})_2$ can be estimated to be $x = 0.63$. Similarly, the maximum solubility of Ca in the C36 Laves phase $Mg(Ni_{0.9}Al_{0.1})_2$ was determined to be $x = 0.76$. Thus the C15 and C36 phases coexist within an approximate composition range of $x = 0.63$–0.76.

Comparing the above results with the reported data for $Ca_{1-x}Mg_xNi_2$ alloys [21], we should note that the composition range for the two-phase region shifted to lower x values because of the partial substitution of Ni by Al. Although Terashita did not report the detailed composition range for the two-phase region in $Ca_{1-x}Mg_xNi_2$ alloys, it was ascertained that the $Ca_{0.32}Mg_{0.68}Ni_2$ alloy contained the single C15 phase and the $Ca_{0.24}Mg_{0.76}Ni_2$ alloy consisted of C15 and C36 [21]. This means that the partial substitution of Ni by Al can stabilize the C36 structure.

Table 1
Structural parameters and phase abundance of the $Ca_{1-x}Mg_x(Ni_{0.9}Al_{0.1})_2$ alloys refined by the X-ray Rietveld analysis

Alloy	Phase	Space group	R_{wp} (%)	S	R_I (%)	Lattice parameters		Abundance (wt%)
						a (Å)	c (Å)	
$x = 0$	C15	$Fd\bar{3}m$	8.18	3.09	4.77	7.2663(4)		100
$x = 0.3$	C15	$Fd\bar{3}m$	9.16	3.94	3.87	7.1206(6)		100
$x = 0.4$	C15	$Fd\bar{3}m$	7.31	3.13	2.62	7.0537(6)		100
$x = 0.5$	C15	$Fd\bar{3}m$	8.76	3.61	3.78	7.0246(2)		100
$x = 0.6$	C15	$Fd\bar{3}m$	7.66	3.25	3.90	6.9757(2)		100
$x = 0.7$	C15	$Fd\bar{3}m$	8.50	3.90	1.08	6.9568(4)		52
	C36	$P6_3/mmc$			1.58	4.8718(5)	15.972(1)	48
$x = 0.8$	C36	$P6_3/mmc$	8.68	4.05	2.40	4.8677(2)	15.963(1)	100
$x = 1$	C36	$P6_3/mmc$	8.26	4.04	1.53	4.8498(4)	15.912(1)	100

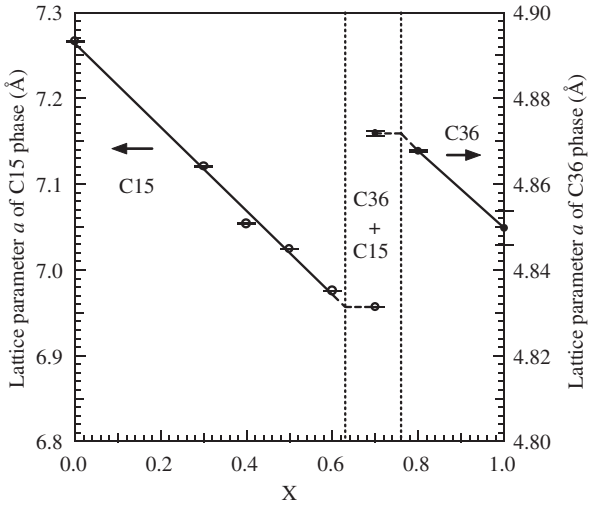

Fig. 5. Relationships between the lattice parameter a of the Laves phases and x in $Ca_{1-x}Mg_x(Ni_{0.9}Al_{0.1})_2$ alloys.

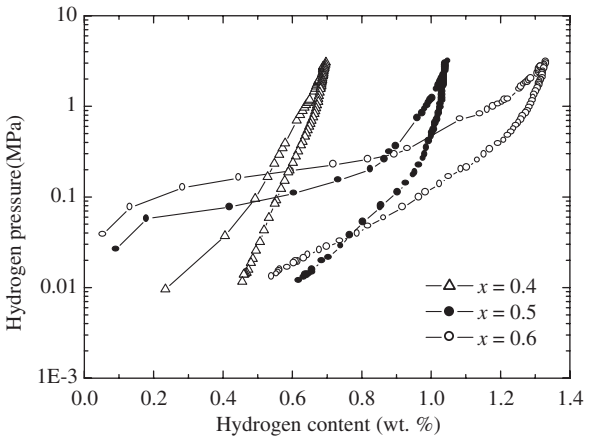

Fig. 6. Pressure–composition isotherms for $Ca_{1-x}Mg_x(Ni_{0.9}Al_{0.1})_2$ ($x = 0.4$, 0.5 and 0.6) alloys at 313 K.

Fig. 6 shows the P–C isotherms of the $Ca_{1-x}Mg_x(Ni_{0.9}Al_{0.1})_2$ ($x = 0.4$, 0.5 and 0.6) alloys at 313 K. It can be seen that there is no obvious pressure plateau for the hydrogen absorption/desorption of the $Ca_{0.6}Mg_{0.4}(Ni_{0.9}Al_{0.1})_2$ alloy. However, the hydrogen absorption/desorption plateaus can be obtained for the $Ca_{0.5}Mg_{0.5}(Ni_{0.9}Al_{0.1})_2$ alloy. Increasing x to 0.6, the hydrogen capacity increases further. The hydrogen absorption capacity of the $Ca_{0.4}Mg_{0.6}(Ni_{0.9}Al_{0.1})_2$ alloy is 1.33 wt%, which is comparable with that of the $Ca_{0.32}Mg_{0.68}Ni_2$ alloy (1.4 wt% [21]). However, the hydrogen desorption capacity of the $Ca_{0.4}Mg_{0.6}(Ni_{0.9}Al_{0.1})_2$ alloy is about 0.8 wt%, which is smaller than that of the $Ca_{0.32}Mg_{0.68}Ni_2$ alloy (1.1 wt% [21]). This indicates that the partial substitution of Ni by Al leads to the decrease of the gaseous hydrogen desorption capacity.

Fig. 7 shows the discharge capacity vs. charging– discharging cycle number for the $Ca_{1-x}Mg_x(Ni_{0.9}Al_{0.1})_2$ ($x = 0.4$, 0.5 and 0.6) alloys at a discharge current of 50 mA/g. It can be seen that the initial discharge capacity of each alloy electrode shows a maximum value. Especially, the $Ca_{0.4}Mg_{0.6}(Ni_{0.9}Al_{0.1})_2$ alloy electrode has a discharge capacity of 365 mAh/g at the discharge current of 50 mA/g. It was suggested that these electrodes do not need activation. However, the discharge capacity decreases quickly with the increase of cycle number. The bad cyclic stability is mainly caused by the corrosion of Ca and Mg in KOH electrolyte solution.

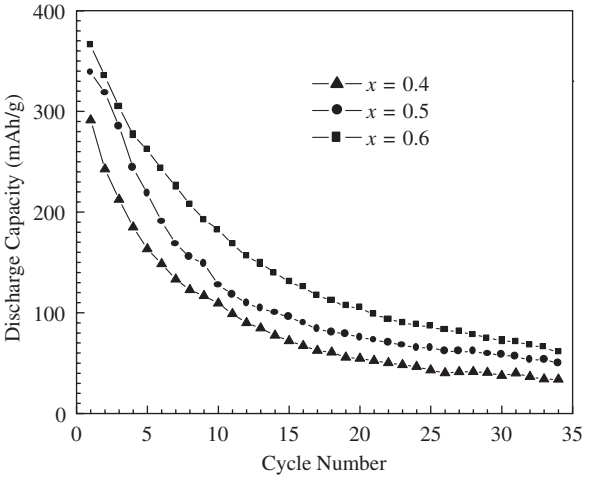

Fig. 7. Discharge capacity at a discharge capacity of 50 mA/g vs. cycle number for $Ca_{1-x}Mg_x(Ni_{0.9}Al_{0.1})_2$ ($x = 0.4$, 0.5 and 0.6) alloys at 298 K.

Fig. 8 shows the initial discharge capacity of the $Ca_{1-x}Mg_x(Ni_{0.9}Al_{0.1})_2$ ($x = 0.4$, 0.5 and 0.6) alloys at different discharge currents. It can be seen that the discharge capacity was enhanced with the increase of x. The discharge capacity of the $Ca_{0.4}Mg_{0.6}(Ni_{0.9}Al_{0.1})_2$ alloy is 401 mAh/g at a discharge current of 10 mA/g, which is larger than $LaNi_5$-based alloys. It is interesting to note that the capacity of the $Ca_{0.4}Mg_{0.6}(Ni_{0.9}Al_{0.1})_2$ alloy is almost same as that of $CaNi_5$-based alloy [25] but larger than that of $CaMg_2Ni_9$ alloy [17].

From the results above, it is certain that the $Ca_{0.4}Mg_{0.6}(Ni_{0.9}Al_{0.1})_2$ alloy with the C15 structure has a high discharge capacity. However, the cyclic stability needs to be improved significantly.

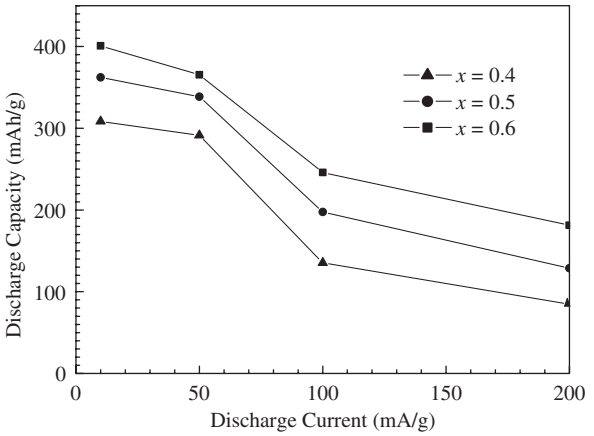

Fig. 8. Relations between discharge capacity and discharge current for $Ca_{1-x}Mg_x(Ni_{0.9}Al_{0.1})_2$ ($x = 0.4$, 0.5 and 0.6) alloys at 298 K.

Thus further work should be done to increase the corrosion resistance of the alloy in KOH electrolyte solution.

4. Conclusions

In the $Ca_{1-x}Mg_x(Ni_{0.9}Al_{0.1})_2$ alloys, the single C15 phase and the single C36 phase exist, respectively, in the approximate composition ranges of $x = 0$–0.63 and 0.76–1. Between the single-phase regions, the C15 and C36 phases coexist. The hydrogen absorption/desorption characteristics and electrochemical properties of the C15-type $Ca_{1-x}Mg_x(Ni_{0.9}Al_{0.1})_2$ alloys are related to Mg content x. There is no obvious pressure plateau for the hydrogen absorption/desorption of the $Ca_{0.6}Mg_{0.4}(Ni_{0.9}Al_{0.1})_2$ alloy at 313 K. Increasing x to 0.6, however, the absorption/desorption plateaus can be obtained and the hydrogen absorption and desorption capacities are 1.33 and 0.8 wt%, respectively. All the alloy electrodes do not need activation during electrochemical measurements. Among these alloys, the $Ca_{0.4}Mg_{0.6}(Ni_{0.9}Al_{0.1})_2$ alloy possesses the highest discharge capacity (about 401 mAh/g) at a discharge current of 10 mA/g. However, the discharge capacity decreases quickly with the increase of cycle number. Further work should be done to increase the corrosion resistance of the alloy in KOH electrolyte solution.

Acknowledgements

This work is supported by National Natural Science Foundation of China (no. 50371001), the Key Project of Chinese Ministry of Education (no. 205070) and the Scientific Research Foundation for the Candidates of Academic Leaders, Education Department of Anhui Province (no. 2005hbz08).

References

[1] Bogdanovic B, Brand RA, Marjanovic A, Schwickardj M, Tolle J. Metal-doped sodium aluminium hydrides as potential new hydrogen storage materials. J Alloys Comp 2000;302:36–58.

[2] Zaluska A, Zaluski L, Strom-Olsen JO. Sodium alanates for reversible hydrogen storage. J Alloys Comp 2000;298:125–34.

[3] Gross KJ, Guthrie S, Takara S, Thomas G. In-situ X-ray diffraction study of the decomposition of $NaAlH_4$. J Alloys Comp 2000;297:270–81.

[4] Jensen CM, Zidan R, Mariels N, Hee A, Hagen C. Advanced titanium doping of sodium aluminum hydride: segue to a practical hydrogen storage material. Int J Hydrogen Energy 1999;24:461–5.

[5] Meisner GP, Tibbetts GG, Pinkerton FE, Olk CH, Balogh MP. Enhancing low pressure hydrogen storage in sodium alanates. J Alloys Comp 2002;337:254–63.

[6] Balema VP, Pecharsky VK, Dennis KW. Solid state phase transformations in $LiAlH_4$ during high-energy ball-milling. J Alloys Comp 2000;313:69–74.

[7] Zhang QA, Nakamura Y, Oikawa K, Kamiyama T, Akiba E. Synthesis and crystal structure of Sr_2AlH_7: a new structural type of alkaline earth aluminum hydride. Inorg Chem 2002;41:6547–9.

[8] Zhang QA, Nakamura Y, Oikawa K, Kamiyama T, Akiba E. New alkaline earth aluminum hydride with one-dimensional zigzag chains of $[AlH_6]$: synthesis and crystal structure of $BaAlH_5$. Inorg Chem 2002;41:6941–3.

[9] Zhang QA, Nakamura Y, Oikawa K, Kamiyama T, Akiba E. Hydrogen-induced phase decomposition of Ba_7Al_{13} and crystal structure of Ba_2AlH_7. J Alloys Comp 2003;361:180–6.

[10] Orimo S, Fujii H. Materials science of Mg-Ni-based new hydrides. Appl Phys A 2001;72:167–86.

[11] Zaluska A, Zaluski L, Strom-Olsen JO. Structure, catalysis and atomic reactions on the nano-scale: a systematic approach to metal hydrides for hydrogen storage. Appl Phys A 2001;72:157–65.

[12] Kadir K, Sakai T, Uehara I. Structural investigation and hydrogen storage capacity of $LaMg_2Ni_9$ and $(La_{0.65}Ca_{0.35})(Mg_{1.32}Ca_{0.68})Ni_9$ of the AB_2C_9 type structure. J Alloys Comp 2000;302:112–7.

[13] Kadir K, Sakai T, Uehara I. Synthesis and structure determination of a new series of hydrogen storage alloys: RMg_2Ni_9 (R = La, Ce, Pr, Nd, Sm and Gd) built from $MgNi_2$ Laves-type layers alternating with AB_5 layers. J Alloys Comp 1997;257:115–21.

[14] Kohno T, Yoshida H, Kawashima F, Inaba T, Sasaki I, Yamamoto K, et al. Hydrogen storage properties of new ternary system alloys: La_2MgNi_9, $La_5Mg_2Ni_{23}$, La_3MgNi_{14}. J Alloys Comp 2000;311:L5–7.

[15] Liao B, Lei YQ, Chen LX, Lu GL, Pan HG, Wang QD. Effect of the La/Mg ratio on the structure and electrochemical properties of $La_xMg_{3-x}Ni_9$ ($x = 1.6$–2.2) hydrogen storage

electrode alloys for nickel–metal hydride batteries. J Power Sources 2004;129:358–67.
[16] Sandrock GD, Murrary JJ, Post ML, Taylor JB. Hydrides and deuterides of $CaNi_5$. Mater Res Bull 1982;17:887–94.
[17] Kadir K, Kuriyama N, Sakai T, Uehara I, Eriksson L. Structural investigation and hydrogen capacity of $CaMg_2Ni_9$: a new phase in the AB_2C_9 system isostructural with $LaMg_2Ni_9$. J Alloys Comp 1999;284:145–54.
[18] Kadir K, Sakai T, Uehara I. Structural investigation and hydrogen capacity of YMg_2Ni_9 and $(Y_{0.5}Ca_{0.5})(MgCa)Ni_9$: new phases in the AB_2C_9 system isostructural with $LaMg_2Ni_9$. J Alloys Comp 1999;287:264–70.
[19] Liang G, Schulz R. Phase structures and hydrogen storage properties of Ca–Mg–Ni alloys prepared by mechanical alloying. J Alloys Comp 2003;356/357:612–6.
[20] Oesterreicher H, Ensslen K, Kerlin A, Bucher E. Hydriding behavior in Ca–Mg–Ni–B. Mater Res Bull 1980;15: 275–83.
[21] Terashita N, Kobayashi K, Sakai T, Akiba E. Structural and hydriding properties of $(Mg_{1-x}Ca_x)Ni_2$ Laves phase alloys. J Alloys Comp 2001;327:275–80.
[22] Izumi F, Ikeda T. A Rietveld-analysis program RIETAN-98 and its applications to zeolites. Mater Sci Forum 2000;321/323: 198–203.
[23] Buschow KHJ. Calcium-nickel intermetallic compounds. J Less-Common Met 1974;38:95–8.
[24] Komura Y, Tokunaga K. Structural studies of stacking variants in Mg-based Friauf-Laves phases. Acta Crystallogr B B 1980;36:1548–54.
[25] Li ZP, Suda S. A new family of hydride electrode materials based on $CaNi_5$-type alloys. J Alloys Comp 1995;231: 751–4.